Polar Effect in Hydrogen Abstraction Reactions from Halo-Substituted Methanes by Methyl Radical: A Comparison between Hartree−Fock, Perturbation, and Density Functional Theories

Fernando Bernardi and Andrea Bottoni*

Dipartimento di Chimica "G. Ciamician", Universita' di Bologna, via Selmi 2, 40126 Bologna, Italy

Received: July 11, 1996; In Final Form: November 15, 1996[⊗]

In this paper we have investigated the hydrogen abstraction reactions by methyl radical from fluoro-, chloro-, and bromomethanes using ab-initio (HF and MP2) and DFT-based methods. The DFT computations have been performed using different functionals, including nonlocal corrections in all cases. At all levels of theory the computational results have shown the following: (i) the reaction proceeds in one step through a transition state which shows a collinear or nearly collinear arrangement of the three atoms involved in the process, (ii) the only relevant effect of dynamic correlation on the geometry of the transition states is increase their reactant-like character (see MP2 and DFT results), (iii) the inclusion of dynamic correlation for reactants and transition states is essential to obtain reasonable values of the computed activation energies, and (iv) the energy barriers computed with the DFT approach are strongly dependent on the type of functional which is used. The best values have been obtained with the hybrid functional B3LYP which provides activation energies which are in better agreement with the experiment than the MP2 values which are in all cases quite overestimated. The present study indicates that the DFT method based on the B3LYP functional is suitable for investigating extensively this class of reactions. A simple diabatic model is used to rationalize the trend of reactivity observed when more halogen atoms are added to the substrate or when the halogen varies from fluorine to chlorine and bromine.

Introduction

The radical abstraction of a hydrogen atom from a substrate represents an important step in the propagation of many chain reactions. A vast amount of experimental work has been carried out to establish and document the general characteristics of these reactions.[1] Many of these studies have pointed out that the rate of radical abstractions are the results of a "complex interplay of polar, steric and bond-strength factors". Tedder, in particular, in a comprehensive review article,[1c] has proposed five useful rules to be used to establish the relative importance of these factors in specific cases. Nevertheless, it seems that no simple property can be used to provide a general qualitative theory which can predict the course of these reactions. In the lack of a simple model capable of rationalizing many of these experimental data, the computational approach can be of great help and the recent progresses of computational chemistry have made possible the use of advanced methods to obtain useful information on the transition state structure and the activation barriers and reaction enthalpies for these processes.[2]

In this paper we focus our attention on the hydrogen abstraction from fluoro-, chloro-, and bromomethanes by methyl radicals:

$$CH_nX_m + {}^{\bullet}CH_3 \rightarrow {}^{\bullet}CH_{n-1}X_m + CH_4$$

where $m = 1$, 2, and 3 and $n = 3$, 2, and 1 for X = F and Cl and $m = 1$ and 2 and $n = 2$ and 1 for X = Br. For these reactions an irregular ordering of the activation energies is observed.[1c] For fluoromethanes, the activation energy decreases on going from CH_3F to CH_2F_2 but increases again for CHF_3. For chloromethanes and bromomethanes the activation energy decreases regularly along the series CH_3Cl, CH_2Cl_2 $CHCl_3$[1b] and $CH_3BrCH_2Br_2$:[1b] in the first case this trend parallels that of the C−H bond energies, while in the second case the trend is opposite.

To investigate these reactions we use the unrestricted Hartree−Fock (UHF) method and the Moller−Plesset perturbation theory up to second order (MP2). It is well-known that the HF method is capable of providing reasonable geometrical parameters for the most part of stable organic molecules and, in many cases (if a single configuration is dominant), also for the transition states, while the activation barriers are usually overestimated. However, the application of ab-initio methods including dynamic correlation (MP2) improves greatly the description and provides, for several reactions, barriers in good agreement with the experiment. Since the cost of correlated ab-initio methods is high and increases rapidly with the increase in size of the molecules, the application of these methods is still limited to rather small systems.

In the last decade much interest has been given to methods that are based on density functional theory (DFT),[3] which appeared as a versatile computational approach capable of successfully describing many problems previously covered exclusively by ab-initio HF and post-HF methods. DFT-based methods have been applied to many types of structural and reactivity problems using, in particular, the form which is known as local density approximation (LDA).[4] These studies have shown that local methods provide geometries which are in better agreement with the experiment than the HF results (in particular for transition metal complexes),[5] even if unsatisfactory results have been found in the calculation of energy barriers and bond energies, which are systematically overestimated.[5] Many of the problems of the local approaches have been eliminated by introducing correction terms based on electron density gradients (nonlocal methods).[6] These corrections improve the evaluation of the exchange and correlation terms in the functional and provide much better results in the computation of

[⊗] Abstract published in *Advance ACS Abstracts,* January 1, 1997.

S1089-5639(96)02068-3 CCC: $14.00

bond energies and in the description of metal−metal and metal−ligands bonds.

Since during the last years only a few papers have appeared where a systematic comparison between traditional correlated ab-initio methods and DFT-based methods has been carried out,[5i−l] we have applied different forms of nonlocal DFT methods to the study of the title reactions. Our purpose is to compare the accuracy of DFT techniques with post-HF methods (like MP2) in computing molecular properties. A calibration of DFT methods for identifying strengths and weaknesses of each functional is now particularly important since this approach has become recently quite popular. This popularity stems in large measure from its computational expedience which makes DFT-based methods particularly suitable for the computations on large-size molecular systems.

Computational Procedure

All the DFT and ab-initio computations reported here were performed with the Gaussian 92/DFT[7] series of programs using the 6-31G* [8a] and the 6-31G** [8b] basis set. For bromine, the polarized split-valence SV4P basis set of Andzelm et al.,[8c] whose accuracy is comparable to that of the 6-31G* basis, was used. In all cases (HF, MP2, and DFT) the geometries of the various critical points were fully optimized with the gradient method available in Gaussian 92. The nature of each critical point was characterized by computing the harmonic vibrational frequencies. As suggested by Sosa and Schlegel,[9] we used spin-projected MP2 energies to cancel the spin contamination, which affects the transition structures and can cause an overestimation of the energy barriers.

For the DFT computations, we have used a pure functional and two hybrid functionals as implemented in Gaussian 92/DFT. Following the Gaussian 92/DFT formalism, these functionals can be written in the general form:

$$a_1E(\mathrm{S})_x + a_2E(\mathrm{HF})_x + a_3E(\mathrm{B88})_x + a_4E(\mathrm{LOCAL})_c + a_5E(\mathrm{NON\text{-}LOCAL})_c \quad (1)$$

where $E(\mathrm{S})_x$ is the Slater exchange,[4a,b] $E(\mathrm{HF})_x$ the Hartree−Fock exchange, $E(\mathrm{B88})_x$ the Becke's 1988 nonlocal exchange functional corrections,[6h] $E(\mathrm{LOCAL})_c$ a local correlation functional, and $E(\mathrm{NON\text{-}LOCAL})_c$ is the gradient-corrected correlation functional. One of the two hybrid functionals that we have used corresponds to the Becke's three-parameter exchange functional[6j] and is denoted here as B3LYP. In this case, $E(\mathrm{LOCAL})_c$ corresponds to the Vosko, Wilk, and Nusair local correlation functional[4d] and $E(\mathrm{NON\text{-}LOCAL})_c$ to the correlation functional of Lee, Yang, and Parr ($E(\mathrm{LYP})_c$)[6f,i] which includes both local and nonlocal terms; the coefficients in expression 1 are those determined by Becke ($a_1 = 0.80$, $a_2 = 0.20$, $a_3 = 0.72$, $a_4 = 0.19$, and $a_5 = 0.81$). The other hybrid method, denoted here as BHLYP, is characterized by the following parameters: $a_1 = 0.50$, $a_2 = 0.50$, $a_3 = 0.50$, $a_4 = 0.00$, and $a_5 = 1.00$.

The pure DFT functional used here, denoted as BLYP, has the following expression:

$$E(\mathrm{S})_x + E(\mathrm{B88})_x + E(\mathrm{LYP})_c \quad (2)$$

which derives from expression 1 assuming $a_1 = a_3 = a_5 = 1.00$, $a_2 = a_4 = 0.00$, and $E(\mathrm{NON\text{-}LOCAL})_c = E(\mathrm{LYP})_c$.

Results and Discussion

A. Structures. A schematic representation of the transition structures corresponding to the hydrogen abstraction from fluoro, chloro and bromomethanes by methyl radical is given in Figure 1. The most relevant geometrical parameters are collected in Tables 1−3. For completeness we have also reported the reactant geometrical parameters in Table 4. The bond lengths and bond angles given in these tables are defined in Figure 1.

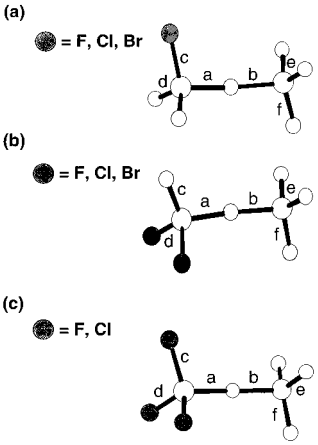

Figure 1. Schematic transition state structures for the reaction $CH_nX_m + {}^{\bullet}CH_3 \rightarrow {}^{\bullet}CH_{n-1}X_m + CH_4$ ($m = 1$, 2, and 3 and $n = 3$, 2, and 1 for X = F and Cl and $m = 1$ and 2 and $n = 2$ and 1 for X = Br).

TABLE 1: Optimum Values[a] of the Most Relevant Geometrical Parameters of the Transition State for the Abstraction Reactions Involving Fluoromethanes Obtained with the 6-31G* and the 6-31G (in Parentheses) Basis Sets at Various Levels of Theory**

	HF	MP2	BHLYP	B3LYP	BLYP
			(a) $CH_3F + {}^{\bullet}CH_3$		
a	1.353	1.319	1.325	1.320 (1.318)	1.320
b	1.360	1.348	1.358	1.388 (1.390)	1.418
c	1.351	1.378	1.354	1.367 (1.368)	1.382
∠*ab*	174.1	169.9	173.5	175.3 (175.3)	177.2
∠*ac*	106.6	105.6	106.9	107.8 (107.9)	108.5
∠*ad*	107.0	107.8	106.9	106.6 (106.5)	106.5
∠*be*	105.1	104.8	104.7	104.5 (104.4)	104.3
∠*bf*	106.0	106.4	106.0	105.6 (105.5)	105.3
θ	0.997	0.977	0.975	0.948 (0.945)	0.927
			(b) $CH_2F_2 + {}^{\bullet}CH_3$		
a	1.356	1.320	1.324	1.316 (1.314)	1.308
b	1.349	1.344	1.354	1.390 (1.393)	1.430
d	1.329	1.357	1.335	1.351 (1.351)	1.368
∠*ab*	175.1	171.7	174.7	175.9 (175.5)	176.8
∠*ac*	110.9	112.5	111.0	110.8 (110.8)	110.8
∠*ad*	107.3	106.8	107.3	107.6 (107.6)	107.9
∠*be*	105.5	105.6	105.3	104.9 (104.8)	104.6
∠*bf*	104.8	104.4	104.5	104.1 (104.0)	103.8
θ	1.010	0.981	0.978	0.944 (0.939)	0.911
			(c) $CHF_3 + {}^{\bullet}CH_3$		
a	1.376	1.349	1.353	1.345 (1.345)	1.337
b	1.322	1.312	1.320	1.351 (1.352)	1.387
c	1.312	1.341	1.321	1.339 (1.339)	1.357
d	1.312	1.341	1.321	1.339 (1.339)	1.357
∠*ab*	180.0	180.0	180.0	180.0 (180.0)	180.0
∠*ac*	109.6	109.8	109.5	109.8 (109.8)	109.6
∠*ad*	109.6	109.8	109.5	109.8 (109.8)	109.6
∠*be*	105.2	105.2	105.1	104.7 (104.6)	104.4
∠*bf*	105.2	105.2	105.1	104.7 (104.6)	104.4
θ	1.049	1.029	1.028	0.995 (0.993)	0.963

[a] Bond lengths are in angstroms and angles in degrees.

In all cases we have found that hydrogen abstraction from halomethanes proceeds in one step and that, in the corresponding transition state, the methyl radical approaches a hydrogen atom of the substrate in a staggered conformation, with the three atoms involved in the process being in a collinear or nearly collinear arrangement. In the case of CHX_3 (X = F and Cl) the transition state has a D_{3d} symmetry while for CH_3X and CH_2X_2 (X = F,

TABLE 2: Optimum Values[a] of the Most Relevant Geometrical Parameters of the Transition State for the Abstraction Reactions Involving Chloromethanes Obtained with the 6-31G* Basis Set at Various Levels of Theory

	HF	MP2	BHLYP	B3LYP	BLYP
			(a) $CH_3Cl + {}^{\bullet}CH_3$		
a	1.354	1.320	1.326	1.323	1.324
b	1.349	1.339	1.348	1.374	1.399
c	1.761	1.753	1.758	1.776	1.797
∠*ab*	178.8	179.0	179.4	179.2	178.0
∠*ac*	108.0	108.3	108.2	108.9	109.5
∠*ad*	106.3	106.2	106.3	106.4	106.5
∠*be*	104.8	104.7	104.5	104.2	104.0
∠*bf*	105.7	105.9	105.6	104.4	105.4
θ	1.000	0.988	0.986	0.966	0.948
			(b) $CH_2Cl_2 + {}^{\bullet}CH_3$		
a	1.348	1.308	1.314	1.303	1.295
b	1.345	1.345	1.355	1.393	1.432
d	1.751	1.750	1.753	1.774	1.798
∠*ab*	178.8	179.1	179.0	180.0	178.7
∠*ac*	106.7	107.1	107.1	107.3	108.0
∠*ad*	107.2	107.2	107.3	107.7	108.0
∠*be*	105.0	104.9	104.7	104.4	104.1
∠*bf*	104.2	103.7	103.5	102.9	102.3
θ	1.011	0.975	0.975	0.940	0.909
			(c) $CHCl_3 + {}^{\bullet}CH_3$		
a	1.343	1.298	1.302	1.287	1.272
b	1.343	1.349	1.361	1.407	1.460
c	1.749	1.753	1.755	1.779	1.807
d	1.749	1.753	1.755	1.779	1.807
∠*ab*	180.0	180.0	180.0	180.0	180.0
∠*ac*	106.1	106.4	106.2	106.6	107.0
∠*ad*	106.1	106.4	106.2	106.6	107.0
∠*be*	104.4	104.0	103.8	103.2	102.6
∠*bf*	104.4	104.0	103.8	103.2	102.6
θ	1.011	0.965	0.964	0.921	0.877

[a] Bond lengths are in angstroms and angles in degrees.

TABLE 3: Optimum Values[a] of the Most Relevant Geometrical Parameters of the Transition State for the Abstraction Reactions Involving Bromomethanes Obtained with the 6-31G* Basis Set at Various Levels of Theory

	HF	MP2	BHLYP	B3LYP	BLYP
			(a) $CH_3Br + {}^{\bullet}CH_3$		
a	1.357	1.331	1.331	1.328	1.326
b	1.343	1.325	1.339	1.365	1.391
c	1.921	1.918	1.914	1.931	1.951
∠*ab*	179.8	179.5	178.8	177.3	176.1
∠*ac*	107.9	107.4	108.3	109.3	110.1
∠*ad*	106.8	107.4	106.8	106.8	106.9
∠*be*	104.8	104.6	104.5	104.1	103.9
∠*bf*	105.9	106.1	105.8	105.7	105.7
θ	1.017	1.006	0.999	0.977	0.958
			(b) $CH_2Br_2 + {}^{\bullet}CH_3$		
a	1.352	1.320	1.317	1.303	1.292
b	1.338	1.328	1.348	1.387	1.427
d	1.911	1.914	1.908	1.929	1.956
∠*ab*	179.4	178.9	179.0	177.6	176.0
∠*ac*	106.7	108.2	107.0	107.1	107.7
∠*ad*	107.3	107.2	107.6	108.2	108.7
∠*be*	105.1	105.0	104.8	104.4	104.0
∠*bf*	104.1	103.5	103.3	102.7	102.0
θ	1.021	0.997	0.992	0.946	0.911

[a] Bond lengths are in angstroms and angles in degrees.

Cl, and Br) the symmetry is reduced to C_s. The transition vector associated with the imaginary frequency is a linear combination of the two breaking and forming C−H bonds (parameters *a* and *b* in Figure 1). These results are in agreement with previous computations performed at a lower level of theory and accuracy.[2e]

We first discuss in detail the abstraction from fluoromethanes. Inspection of the results obtained at the HF level shows that

TABLE 4: Optimum Values[a] of the Most Relevant Geometrical Parameters for the Methyl Radical and the Various Halo-Substituted Methanes Obtained with the 6-31G* and the 6-31G (in Parentheses) Basis Sets at Various Levels of Theory**

	HF	MP2	BHLYP	B3LYP	BLYP
			(a) ${}^{\bullet}CH_3$[b]		
e	1.073	1.079	1.075	1.083 (1.082)	1.090
			(b) CH_3F		
a	1.082	1.092	1.086	1.097 (1.096)	1.105
c	1.364	1.392	1.369	1.383 (1.383)	1.398
d	1.082	1.092	1.086	1.097 (1.096)	1.105
∠*ac*	109.1	109.1	109.4	109.6 (109.7)	109.7
∠*ad*	109.8	109.8	109.5	109.3 (109.2)	109.2
			(c) CH_2F_2		
a	1.078	1.091	1.085	1.096 (1.096)	1.105
c	1.078	1.091	1.085	1.096 (1.096)	1.105
d	1.338	1.366	1.345	1.361 (1.361)	1.377
∠*ac*	112.4	112.8	112.3	112.2 (112.1)	112.2
∠*ad*	108.9	108.8	108.9	108.9 (108.9)	108.8
			(d) CHF_3		
a	1.074	1.089	1.082	1.093 (1.094)	1.102
c	1.316	1.344	1.325	1.342 (1.342)	1.359
d	1.316	1.344	1.325	1.342 (1.342)	1.359
∠*ac*	110.4	110.5	110.4	110.4 (110.4)	110.4
∠*cd*	108.5	108.4	108.5	108.6 (108.6)	108.6
			(e) CH_3Cl		
a	1.078	1.088	1.081	1.090	1.097
c	1.784	1.779	1.784	1.804	1.826
d	1.078	1.088	1.081	1.090	1.097
∠*ac*	108.5	108.9	108.6	108.5	108.3
∠*ad*	110.4	110.0	110.3	110.4	110.6
			(f) CH_2Cl_2		
a	1.074	1.087	1.079	1.088	1.095
c	1.074	1.087	1.079	1.088	1.095
d	1.768	1.769	1.771	1.791	1.814
∠*ac*	111.1	110.8	111.1	111.5	112.1
∠*ad*	108.2	108.2	108.1	108.0	107.8
			(g) $CHCl_3$		
a	1.071	1.086	1.076	1.085	1.093
c	1.763	1.766	1.767	1.788	1.811
d	1.763	1.766	1.767	1.788	1.811
∠*ac*	107.6	107.6	107.6	107.5	107.5
∠*cd*	111.3	111.2	111.3	111.3	111.3
			(h) CH_3Br		
a	1.076	1.087	1.080	1.088	1.095
c	1.947	1.947	1.941	1.960	1.986
d	1.076	1.087	1.080	1.088	1.095
∠*ac*	111.2	111.2	111.1	111.2	111.4
∠*ad*	107.7	107.6	107.8	107.6	107.4
			(i) CH_2Br_2		
a	1.072	1.086	1.077	1.086	1.093
c	1.072	1.086	1.077	1.086	1.093
d	1.928	1.933	1.933	1.945	1.972
∠*ac*	111.9	112.3	111.9	112.3	113.0
∠*ad*	107.9	107.8	107.8	107.7	107.4

[a] Bond lengths are in angstroms and angles in degrees. [b] The ${}^{\bullet}CH_3$ radical is planar at all levels of theory.

the transition state slightly advances toward the products when more fluorine atoms are introduced in the substrate. The variation of character of the transition state is conveniently described by the quantity $\theta = \delta R(C-H)/\delta R(C-H')$ where $\delta R(C-H) = a/R(C-H)_{eq}$ and $\delta R(C-H') = b/R(C-H')_{eq}$. Here *a* and *b* are the lengths of the breaking and forming C−H bonds, respectively, and $R(C-H)_{eq}$ and $R(C-H')_{eq}$ are the corresponding equilibrium distances in the reactant (halomethane, see Table 4) and product (methane).[10] A value of 1 for θ indicates a transition state where the two bonds are broken and formed to the same extent; a value lower or greater than unity corresponds to a more reactant-like or to a more product-like transition state,

respectively. In the present case, θ varies only slightly (from 0.997 to 1.010) on passing from CH_3F to CH_2F_2 but becomes 1.049 for CHF_3. A slight deviation from linearity has been observed for CH_3F and CH_2F_2 where the $\angle ab$ angle is 174.1° and 175.1°, respectively. The inclusion of dynamic correlation at the MP2 level has the effect of making both the breaking and forming C−H bonds shorter. However, since the shortening is more significant for the breaking bond (*a*) than for the forming bond (*b*), the transition state becomes more reactant-like (decrease of θ). A similar effect has been found at the DFT level. With all three functionals used here we have a significant decrease of the parameter θ with respect to the HF value. The value of this parameter computed with the BHLYP functional is almost identical to the value obtained at the MP2 level, but becomes significantly smaller with the B3LYP and the BLYP functional according to the increasing importance of the correlation term (see expressions 1 and 2). Another effect due to the inclusion of the dynamic correlation is a lengthening of the C−F bonds: the increase of this bond length at the MP2 level is similar to that found at the B3LYP and BLYP levels while it is less significant when the hybrid BHLYP functional is used. Furthermore, it is interesting to note that, also at a correlated level of theory, the character of the transition state is again very similar for CH_3F and CH_2F_2 and becomes much more product-like for CHF_3.

For the three fluoromethanes we have reinvestigated the reaction at the B3LYP level of theory using the more accurate 6-31G** basis to establish the importance of 2p polarization functions on hydrogens. This computational level provides in all cases transition state geometries which are almost identical to those determined with the 6-31G* basis. These results indicate that polarization functions are not essential to obtain a proper description of the topology of the surface as already pointed out.[2h]

Similar results have been obtained for chloro- and bromomethanes. However the inclusion of more chlorine and bromine atoms in the substrate has an opposite effect to that found for fluoromethanes, and the reactant-like character of the transition state increases instead of decreasing along the two series CH_3Cl, $CH_2Cl_2CHCl_3$ and $CH_3BrCH_2Br_2$. Also, for these two series of halomethanes, the inclusion of dynamic correlation is responsible of an increase of the reactant-like character of the transition structure.

B. Energetics. The energies of reactants and transition structures are reported in Table 5. In this table we have also given the values of the zero-point energy corrections (ZPE), the experimental activation energies ($E_{a,exp}$), and the computed activation energies (E_a), which include the ZPE corrections. The accurate prediction of the energy barriers of radical reactions is a difficult problem and it is well-known that high levels of theory including dynamic correlation are needed to reproduce the experimental results.[9] Thus it is not surprising that the activation barriers obtained at the HF level are in all cases overestimated. A large decrease of the energy barriers is observed when the projected MP2 approach is used even if the values obtained at this level of theory are still quite overestimated (the error with respect to the experimental values is in all cases larger than 55%). It is interesting to note that, even if the values are largely overestimated, the irregular ordering of the activation energies as more fluorine atoms are introduced in methane is better reproduced at the HF level than at the MP2 level: at this level of theory the activation energy for CHF_3 (20.82 kcal/mol) is slightly lower than that obtained for CH_3F (21.48 kcal/mol) in contrast with the experiment.

The values of the energy barriers provided by the DFT approach vary significantly according to the type of functional which is used. The BHLYP functional still overestimates the activation barriers, even if the trend in the comparison between CHF_3 (16.04 kcal/mol) and CH_3F (15.77 kcal/mol) is now in agreement with the experiment. Furthermore, the pure DFT functional BLYP provides E_a values which are quite underestimated. The best agreement with the experiment is found for the values computed at the B3LYP level of theory. In this case the difference between the experimental and the corresponding computed E_a values is for all substrates within 1.5 kcal/mol (except for CHF_3), even if the trend differs from the experimental one in that the activation barrier for CHF_3 (10.31 kcal/mol) is slightly smaller than the value determined for CH_3F (10.71 kcal/mol). It is also interesting to note that the inclusion of polarization functions on hydrogens (6-31G** basis set) for the series CH_3F, CH_2F_2, and CHF_3 does not improve the computed E_a values which slightly decrease.

Finally, it is worth comparing the values of $\langle S^2 \rangle$ (see Table 6) computed for the various transition states at the MP2 and DFT (B3LYP) levels. At the MP2 level we have reported the magnitude of $\langle S^2 \rangle$ for both $\Psi^{(0)}$ ($\langle S^2 \rangle_0$) and $\Psi^{(1)}$ ($\langle S^2 \rangle_1$). Inspection of Table 6 shows that the B3LYP functional provides better results than MP2 and points out once again that the DFT approach can significantly reduce the effects of spin contamination.

C. Diabatic Model. In the introductory section we have already pointed out that the dependence of the activation energies on the degree of halogenation of methane cannot be easily explained in terms of simple properties such as the energy of the breaking bond, polar factors, and steric factors. If we consider, for instance, the series CH_3F, CH_2F_2, and CHF_3, where the steric effects are expected to be small, the irregular ordering of the activation energies (see Table 5) does not parallel either the trend of the energy of the C−H breaking bond (which is about 101 kcal/mol for fluoro- and difluoromethane and becomes 106 kcal/mol for trifluoromethane as reported in Table 7) or the trend of the polar effects which increase with the increase in the number of fluorine atoms. Similarly, for the two bromomethanes, the activation energy decreases on passing from CH_3Br to CH_2Br_2 in contrast with the trend of the C−H bond energy which increases in the same direction (see Table 7).

In this section we try to rationalize these trends using a simple diabatic model based upon spin recoupling in VB theory:[12] we show that this approach, if combined with the results of ab-initio computations, can predict easily, even if qualitatively, the main features of this class of reactions (i.e., information on the transition state structures and on the trends of the activation energies). In this model, the total energy profile is decomposed into two component curves: one, associated with the reactant spin coupling (reactant bonding situation), is indicated as *reactant diabatic* and the other, associated with the product spin coupling (product bonding situation), is denoted as *product diabatic*. Along the reaction coordinate the behavior of the reactant diabatic is repulsive and that of the product diabatic is attractive.

In Figure 2 we have represented the qualitative behavior of the two diabatics for the abstraction reaction of a hydrogen from fluoro- (Figure 2a), chloro- (Figure 2b), and bromomethanes (Figure 2c). The reactant diabatic corresponds to a situation where the pσ orbital on the carbon atom of halomethane and the 1s orbital on hydrogen are singlet spin coupled (see reactant coupling in Scheme 1), while in the product diabatic the singlet

TABLE 5: Total (E, hartrees) and Relative (ΔE, kcal/mol) Energies of Reactants and Transition States, Activation Energies (E_a, kcal/mol), and Zero-Point Energy Corrections (ZPE, kcal/mol) Computed for the Abstraction Reaction $CH_nX_m + {}^\bullet CH_3 \rightarrow {}^\bullet CH_{n-1}X_m + CH_4$ ($m = 1$, 2, and 3 and $n = 3$, 2, and 1 for X = F and Cl and $m = 1$ and 2 and $n = 2$ and 1 for X = Br) with the 6-31G* and the 6-31G (Values in Parentheses) Basis Sets at Various Levels of Theory; for Each Reaction the Experimentally Available Activation Energy ($E_{a,exp}$ kcal/mol) Is Reported**

	HF	MP2	BHLYP	B3LYP	BLYP
			(a) $CH_3F + {}^\bullet CH_3$ ($E_{a,exp} = 11.8$ kcal/mol)[d]		
reactants					
E	−178.59361	−179.01336	−179.47796	−179.57219 (−179.58116)	−179.49912
ZPE	46.06	44.59	45.00	43.50 (43.35)	42.30
transition state					
E	−178.54710	−178.97834	−179.45211	−179.55437 (−179.56413)	−179.48630
ZPE	45.73	44.10	44.55	43.04 (42.82)	41.80
ΔE	29.18	21.97	16.22	11.18 (10.68)	8.03
E_a	28.85	21.48	15.77	10.71 (10.15)	7.53
			(b) $CH_2F_2 + {}^\bullet CH_3$ ($E_{a,exp} = 10.4$ kcal/mol)[a]		
reactants					
E	−277.45534	−278.03480	−278.68682	−278.81143 (−278.81893)	−278.73766
ZPE	42.01	40.41	40.93	39.45 (39.31)	38.24
transition state					
E	−277.40872	−.278.00776	−278.66213	−278.79553 (−278.80403)	−278.72725
ZPE	41.31	39.59	40.08	38.59 (38.40)	37.36
ΔE	29.24	16.97	15.49	9.98 (9.35)	6.53
E_a	28.54	16.15	14.64	9.12 (8.44)	5.65
			(c) $CHF_3 + {}^\bullet CH_3$ ($E_{a,exp} = 13.6$ kcal/mol)[a]		
reactants					
E	−376.33063	−377.07784	−377.90965	−378.06426 (−378.07030)	−377.98929
ZPE	37.08	35.56	36.12	34.76 (34.65)	33.61
transition state					
E	−376.28116	−377.04854	−377.88247	−378.04625 (−378.05338)	−377.97708
ZPE	36.17	34.51	35.10	33.76 (33.61)	32.62
ΔE	31.04	18.38	17.05	11.30 (10.61)	7.66
E_a	30.13	17.33	16.03	10.31 (9.57)	6.67
			(d) $CH_3Cl + {}^\bullet CH_3$ ($E_{a,exp} = 9.4$ kcal/mol)[b]		
reactants					
E	−538.65214	−539.02531	−539.87274	−539.94682	−539.86342
ZPE	44.97	43.74	44.02	42.64	41.52
transition state					
E	−538.60672	−538.99893	−539.84754	−539.92905	−539.85010
ZPE	44.74	43.26	43.64	42.23	41.08
ΔE	28.50	16.55	15.80	11.15	8.36
E_a	28.27	16.07	15.42	10.75	7.92
			(e) $CH_2Cl_2 + {}^\bullet CH_3$ ($E_{a,exp} = 7.2$ kcal/mol)[b]		
reactants					
E	−997.54417	−998.04675	−999.44943	−999.53466	−999.44101
ZPE	39.54	38.38	38.63	37.32	36.25
transition state					
E	−997.50217	−998.02585	−999.42864	−999.52155	−999.43248
ZPE	39.13	37.75	38.07	36.73	35.62
ΔE	26.35	13.11	13.04	8.23	5.35
E_a	25.94	12.49	12.48	7.64	4.72
			(f) $CHCl_3 + {}^\bullet CH_3$ ($E_{a,exp} = 5.8$ kcal/mol)[b]		
reactants					
E	−1456.42870	−1457.06511	−1459.02019	−1459.11740	−1459.01409
ZPE	33.24	32.27	32.43	31.25	30.26
transition state					
E	−1456.39042	−1457.04953	−1459.00363	−1459.10846	−1459.00972
ZPE	32.80	31.63	31.82	30.58	29.55
ΔE	24.02	9.78	10.39	5.61	2.74
E_a	23.60	9.14	9.78	4.94	2.03
			(g) $CH_3Br + {}^\bullet CH_3$ ($E_{a,exp} = 10.1$ kcal/mol)[c]		
reactants					
E	−2649.31033	−2649.81091	−2651.57187	−2651.67506	−2651.61143
ZPE	44.52	43.26	43.60	42.22	41.07
transition state					
E	−2649.26431	−2649.78334	−2651.54604	−2651.65644	−2651.59717
ZPE	44.27	42.77	43.25	41.89	40.77
ΔE	28.87	17.29	16.20	11.68	8.94
E_a	28.62	16.80	15.86	11.35	8.64
			(h) $CH_2Br_2 + {}^\bullet CH_3$ ($E_{a,exp} = 8.7$ kcal/mol)[b]		
reactants					
E	−5218.85875	−5219.61755	−5222.84643	−5222.99036	−5222.93649
ZPE	38.61	37.38	37.76	36.44	35.31
transition state					
E	−5218.81627	−5219.59646	−5222.82524	−5222.97678	−5222.92757
ZPE	38.21	36.73	37.21	35.88	34.74
ΔE	26.66	13.23	13.29	8.51	5.59
E_a	26.26	12.58	12.74	7.95	5.02

[a] See ref 1c. [b] See ref 1b.

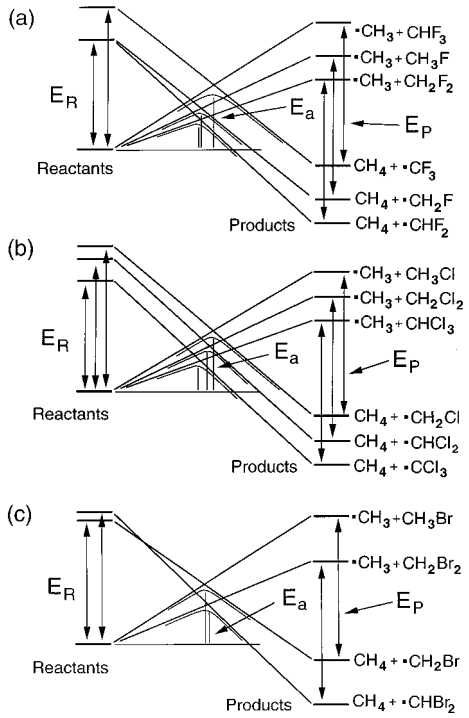

Figure 2. Correlation diagram for hydrogen abstraction from (a) fluoro-, (b) chloro-, and (c) bromomethanes by methyl radical.

TABLE 6: Values of $\langle S^2 \rangle$ Computed at the HF, MP2, and B3LYP Levels with the 6-31G* Basis Set

	MP2		
	$\Psi^{(0)}$	$\Psi^{(1)}$	B3LYP
$CH_3F + \cdot CH_3$	0.7890	0.7629	0.7571
$CH_2F_2 + \cdot CH_3$	0.7885	0.7627	0.7570
$CHF_3 + \cdot CH_3$	0.7882	0.7624	0.7569
$CH_3Cl + \cdot CH_3$	0.7888	0.7629	0.7571
$CH_2Cl_2 + \cdot CH_3$	0.7879	0.7627	0.7669
$CHCl_3 + \cdot CH_3$	0.7861	0.7621	0.7566
$CH_3Br + \cdot CH_3$	0.7896	0.7634	0.7572
$CH_2Br_2 + \cdot CH_3$	0.7891	0.7636	0.7570

TABLE 7: Total Energies (*E*, hartrees) Obtained with the B3LYP Functional and the 6-31G* Basis Set and Corresponding Stabilization Energies (SE, kcal/mol) Computed According to the Homodesmic Reaction 3. For Each Radical[a] the Experimental C−H Bond Energy (BE, kcal/mol) of the Corresponding Halo-Substituted Methane Is Reported

	E	SE	BE
$\cdot CH_2F$	−139.06425	−6.55	101[b]
$\cdot CHF_2$	−238.30552	−7.82	101[b]
$\cdot CF_3$	−337.55102	−3.22	106[c]
$\cdot CH_2Cl$	−499.43829	−6.18	100.9[d]
$\cdot CHCl_2$	−959.03406	−11.16	99.0[d]
$\cdot CCl_3$	−1418.62331	−15.25	95.8[e]
$\cdot CH_2Br$	−2611.16495	−5.18	102.0[d]
$\cdot CHBr_2$	−5182.48915	−10.77	103.7[d]

[a] Optimum geometrical parameters for the various product radicals are as follows (angstroms and degrees): $\cdot CH_2F$, $c = 1.342$, $d = 1.085$, $\angle cd = 114.9$, $\angle dd = 122.9$; $\cdot CHF_2$, $c = 1.093$, $d = 1.333$, $\angle cd = 113.8$, $\angle dd = 111.6$; $\cdot CF_3$, $c = 1.327$, $\angle cd = 111.3$; $\cdot CH_2Cl$, $c = 1.714$, $d = 1.080$, $\angle cd = 117.7$, $\angle dd = 124.1$; $\cdot CHCl_2$, $c = 1.083$, $d = 1.720$, $\angle cd = 116.7$, $\angle dd = 119.3$; $\cdot CCl_3$, $c = 1.731$, $\angle cd = 116.8$; $\cdot CH_2Br$, $c = 1.868$, $d = 1.080$, $\angle cd = 117.2$, $\angle dd = 124.0$; $\cdot CHBr_2$, $c = 1.083$, $d = 1.872$, $\angle cd = 115.8$, $\angle dd = 120.8$. [b] See ref 11a. [c] See ref 11b. [d] See ref 11c. [e] See ref 11d.

spin coupling occurs between the 1s hydrogen orbital and the pσ orbital on the methyl radical carbon (see product coupling in Scheme 1).

SCHEME 1

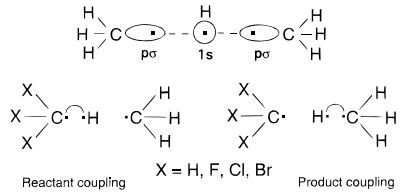

The relative energy position of reactants and products in the diagrams of Figure 2 can be determined on the basis of the stabilization (or destabilization) of the $\cdot CH_{n-1}X_m$ radical with respect to the methyl radical. This stabilization (SE) can be easily computed for a $\cdot CH_{n-1}X_m$ radical according to the following homodesmic reaction:

$$\cdot CH_3 + CH_nX_m \rightarrow CH_4 + \cdot CH_{n-1}X_m \qquad (3)$$

and is given by

$$SE = [E_t(CH_4) + E_t(\cdot CH_{n-1}X_m)] - [E_t(\cdot CH_3) + E_t(CH_nX_m)] \qquad (4)$$

where E_t represents the total energy obtained at the ab-initio level. Negative values of SE mean that the $\cdot CH_{n-1}X_m$ radical is more stable than the $\cdot CH_3$ radical; positive values mean the reverse. The SE values computed at the B3LYP level for the various fluoro-, chloro-, and bromomethyl radicals are collected in Table 7. These values, which are all negative, show that, for X = Cl and Br, the stabilization increases with the increase in the number of halogen atoms, while for X = F, the stabilization increases on passing from $\cdot CH_2F$ to $\cdot CHF_2$, then decreases for $\cdot CF_3$.

The SE values obtained in this way have been used to construct the three diagrams of Figure 2 which are based on the following considerations: (i) The product diabatics at the product geometry are positioned with respect to the reactant diabatics at the reactant geometry on the basis of the computed SE values. (ii) A common reference energy level for reactants has been assumed in all three cases. (iii) The energy difference between reactant diabatic and product diabatic at the product geometry (ΔE_P on the right side of the diagram) can be assumed to be identical in all cases, since it depends only on the coupling−decoupling between the 1s hydrogen orbital and the pσ carbon orbital in methane and there is no interaction involving the $\cdot CH_{n-1}X_m$ radical which is at infinite separation. More precisely, the total energy of the system at the product geometry contains a constant term corresponding to the energy of the $\cdot CH_{n-1}X_m$ radical which is canceled out in the difference between the energy of the reactant diabatic and that of the product diabatic. (iv) The energy difference between the two diabatics at the reactant geometry (ΔE_R on the left side of the diagram) depends on the coupling−decoupling between the 1s hydrogen orbital and the pσ carbon orbital in CH_nX_m and can be evaluated to a good approximation from the energies of the C−H breaking bond in the various halomethanes (see the BE values in Table 7).

This model allows to discuss the combined effect of the key factors that control the reactivity of these species, i.e., the stability of the radical formed in the reaction and the energy of the C−H breaking bonds.

Inspection of Figure 2 gives the following indications: (a) For fluoromethanes the trend of the activation energies derived from the diagram of Figure 2a is the following:

$$E_a(CHF_3) > E_a(CH_3F) > E_a(CH_2F_2)$$

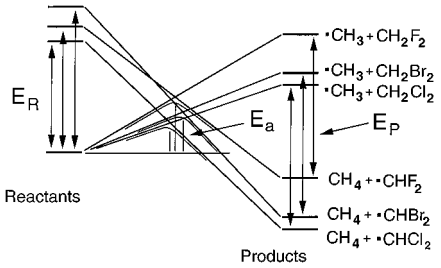

Figure 3. Correlation diagram for hydrogen abstraction from CH_2F_2, CH_2Cl_2, and CH_2Br_2 by methyl radical.

which is in agreement with the experimental observed trend. This trend is determined, in the comparison between CH_3F and CH_2F_2, by the radical stability factor since the energy of the C−H breaking bond is the same (about 101 kcal/mol in both cases), while for CHF_3 both factors (stability and bond energy) concur to increase the activation energy. The diagram also provides information about the geometrical features of the transition state; in particular, the structure of the transition state must be very similar for the reactions involving CH_3F and CH_2F_2 (the position of the crossing does not change significantly) and must be more product-like for CHF_3 (the crossing moves to the right). These predictions are in agreement with the values of the θ coefficient which, at the B3LYP level, is 0.948 and 0.945 for CH_3F and CH_2F_2, respectively, and becomes 0.995 for CHF_3. (b) A similar discussion can be applied to chloro- and bromomethanes. For these species the trends of activation energies derived from the diagrams of Figures 2b and 2c are

$$E_a(CH_3Cl) > E_a(CH_2Cl_2) > E_a(CHCl_3)$$

and

$$E_a(CH_3Br) > E_a(CH_2Br_2)$$

These trends again agree very well with the trends experimentally observed. In the first case (chloromethanes), both factors (radical stability and C−H bond energy) concur to determine the trend, as well as the structural features of the transition state, which becomes more reactant-like as more chlorine atoms are included in the substrate (the value of θ at the B3LYP level is 0.966, 0.940, and 0.921 for CH_3Cl, CH_2Cl_2, and $CHCl_3$, respectively). In the second case, (bromomethanes) the observed trend is determined by the radical stability: even if the C−H bond energy slightly increases from bromomethane to dibromomethane, the radical stability increases more significantly and determines a lowering of the activation energy.

The diabatic model can also rationalize the change in reactivity on passing from fluoro- to chloro- and bromomethanes. To illustrate this aspect, a diabatic diagram, where we compare CH_2F_2, CH_2Cl_2, and CH_2Br_2, is shown in Figure 3. The diagram correctly predicts the irregular ordering of the activation barrier on passing from fluorine to chlorine and bromine, i.e., the smallest activation barrier for CH_2Cl_2 and the largest activation barrier for CH_2F_2. On the basis of this diagram, the transition state for CH_2Cl_2 must be more reactant-like than for CH_2F_2 and CH_2Br_2. This prediction is in agreement with the values of the θ parameter which, at the B3LYP level, are 0.940 for CH_2Cl_2 and 0.944 and 0.946 for CH_2F_2 and CH_2Br_2, respectively. It is interesting to point out that that in this case, the diabatic model can correctly predict the change in the transition state structure while the Hammond postulate fails. On the basis of the relative exothermicities of the three reactions, the Hammond postulate would predict for CH_2F_2 a more product-like transition state than the transition states for CH_2Cl_2 and CH_2Br_2, in disagreement with the computational results. The better performance of the diabatic model depends on the fact that, in determining the position of the transition state, this model can take into account not only the reaction enthalpies but also other factors as the energies of the forming and breaking bonds. Thus only when the trend of these additional factors parallels that of the reaction enthalpies (for example, a larger bond energy corresponding to a lower stability of the resulting radical) or when the reaction enthalpy is the dominating factor can the two models provide the same answer.

Conclusion

In this paper we have reported the results of a comprehensive theoretical study of the hydrogen abstraction reactions by methyl radical from fluoro, chloro and bromomethanes. The study compares the results of traditional ab-initio methods (HF and MP2) with those obtained with DFT-based methods and with the experiment. For the DFT computations we have used a pure functional and two hybrid functionals which include in all cases nonlocal corrections. At all levels of theory we have found that the reaction proceeds in one step through a transition state which shows a collinear or nearly collinear arrangement of the three atoms involved in the process.

These computations have shown the following. (i) The only relevant effect of the inclusion of the dynamic correlation (MP2 and DFT level) on the geometry of the transition states is that of increasing their reactant-like character. This effect is similar at the MP2 and BHLYP level but becomes more important with the B3LYP and the BLYP functionals in agreement with the increasing importance of the correlation term in expressions 1 and 2. (ii) Only negligible changes in the transition state geometries and activation energies have been found using the 6-31G** basis set; this indicates that additional polarization functions on hydrogens are not essential to obtain a reliable description of these reactions. (iii) The inclusion of dynamic correlation for reactants and transition states is essential, as already pointed out,[2e] to obtain reasonable values of the computed activation energies. (iv) The energy barriers computed with the DFT approach are strongly dependent on the type of functional which is used. The best values have been obtained with the hybrid functional B3LYP which provides activation energies which are in better agreement with the experiment than the corresponding MP2 values, which are in all cases quite overestimated. (v) The DFT approach can improve significantly the wave function by reducing the effect of spin contamination as indicated by the $\langle S^2 \rangle$ values.

These results suggest that, if a suitable calibration is chosen, DFT-based methods can provide better energetics than traditional correlated methods (as Moller−Plesset perturbation theory) even if the geometrical results are very similar. The calibration performed here suggests that the B3LYP functional can be used extensively to investigate this class of reactions.

Finally, we have demonstrated that the various results can be rationalized using a simple diabatic model which can be derived from the results of reliable quantum-mechanical computations on reactants and products and from easily available experimental data such as bond energies. This model detects in the bond energies of the breaking and forming C−H bonds and in the different stabilities of the resulting radicals (computed using a homodesmic equation and quantum-mechanical total energies) the key factors which determine the trend of reactivity observed for the various methane derivatives as well as the change of the transition state character when more halogen

atoms are included in the substrate or when the halogen varies from fluorine to chlorine and bromine.

References and Notes

(1) (a) Ruchardt, C. *Angew. Chem., Int. Ed. Engl.* **1970**, *9*, 830. (b) Russel, G. A. *Free Radicals*; Kochi, J. K., Ed.; John Wiley & Sons, Inc.: New York, 1973; Vol. 1. (c) Tedder, J. M. *Angew. Chem., Int. Ed. Engl.* **1982**, *21*, 401.

(2) (a) Dewar, M. J. S.; Haselbach, E. *J. Am. Chem. Soc.* **1970**, *92*, 590. (b) Rayez-Meaume, M. T.; Dannenberg, J. J.; Whitten, J. L. *J. Am. Chem. Soc.* **1978**, *100*, 747. (c) Canadell, E.; Olivella, S.; Poblet, J. M. *J. Phys. Chem.* **1984**, *88*, 3545. (d) Sana, M.; Leroy, G.; Villaveces, J. L. *Theor. Chim. Acta* **1984**, *65*, 109. (e) Wunsch, E.; Lluch, J. M.; Oliva, A.; Bertran, J. *J. Chem. Soc., Perkin Trans. 1* **1987**, *2*, 211. (f) Wunsch, E.; Lluch, J. M.; Oliva, A.; Bertran, J. *J. Chim. Phys.* **1987**, *84*, 769. (g) Fox, G. L.; Schlegel, H. B. *J. Phys. Chem.* **1992**, *96*, 298. (h) Bottoni, A.; Poggi, G.; Emmi, S. *J. Mol. Struct. (THEOCHEM)* **1993**, *279*, 299. (i) Chen, Y.; Tschuikow-Roux, E. *J. Phys. Chem.* **1993**, *97*, 3742. (j) Bottoni, A.; Poggi, G. *J. Mol. Struct. (THEOCHEM)* **1995**, *337*, 161.

(3) Parr, R. G.; Yang, W. *Density-Functional Theory of Atoms and Molecules*; Oxford University Press: New York, 1989.

(4) (a) Hohenberg, P.; Kohn, W. *Phys. Rev.* **1964**, *B136*, 864. (b) Kohn, W.; Sham, L. J. *Phys. Rev.* **1965**, *A140*, 1133. (c) Gunnarson, O.; Lundquist, I. *Phys. Rev.* **1974**, *B10*, 1319. (d) Vosko, S. H.; Wilk, L.; Nusair, M. *Can. J. Phys.* **1980**, *58*, 1200. (e) Perdew, J. P.; Zunger, A. *Phys. Rev.* **1981**, *B23*, 5048. (f) Tschinke, V; Ziegler, T. *Can. J. Chem.* **1989**, *67*, 460.

(5) (a) Versluis, L.; Ziegler, T. *J. Chem. Phys.* **1988**, *88*, 322. (b) Fan, L.; Versluis, L.; Ziegler, T.; Baerends, E. J.; Ravenek, W. *Int. J. Quantum Chem.* **1988**, *S22*, 173. (c) Harris, J.; Jones, R. O.; Muller, J. E. *J. Chem. Phys.* **1981**, *75*, 3904. (d) Fournier, R.; Andzelm, J.; Salahub, D. R. *J. Chem. Phys.* **1989**, *90*, 6371. (e) Delley, B. *J. Chem. Phys.* **1991**, *94*, 7245. (f) Hohl, D.; Jones, R. O.; Car, R.; Parrinello, M. *J. Chem. Phys.* **1988**, *89*, 6823. (g) Jones, R. O.; Hohl, D. *J. Chem. Phys.* **1990**, *92*, 6710. (h) Sim, F.; Salahub, D. R.; Depuis, M. *J. Chem. Phys.* **1991**, *95*, 6050. (i) Fitzgerald, G.; Andzelm, J. *J. Phys. Chem.* **1991**, *95*, 10531. (j) Ziegler, T. *Chem. Rev.* **1991**, *91*, 651. (k) Fan, L.; Ziegler, T. *J. Am. Chem. Soc.* **1992**, *114*, 10890. (l) Bottoni, A. *J. Chem. Soc., Perkin Trans. 2* **1996**, 2041.

(6) (a) Langreth, D. C.; Mehl, M. *Phys. Rev.* **1983**, *B28*, 1809. (b) Becke, A. D. *Int. J. Quantum Chem.* **1983**, *27*, 1915. (c) Becke, A. D. *J. Chem. Phys.* **1986**, *84*, 4524. (d) Perdew, J. P. *Phys. Rev.* **1986**, *B33*, 8822. (e) Becke, A. D. *Phys. Rev.* **1988**, *A33*, 2786. (f) Lee, C.; Yang, W.; Parr, R. G. *Phys. Rev.* **1988**, *B37*, 785. (g) Becke, A. D. *Int. J. Quantum Chem.* **1989**, *S23*, 599. (h) Becke, A. D. *Phys. Rev.* **1988**, *A38*, 3098. (i) Miehlich, A.; Savin, A.; Stoll, H.; Preuss, H. *Chem. Phys. Lett.* **1989**, *157*, 200. (j) Becke, A. D. *J. Chem. Phys.* **1993**, *98*, 5648.

(7) Gaussian 2/DFT, Revision G. 1: M. J. Frisch, G. W. Trucks, H. B. Schlegel, P. M. W. Gill, B. G. Johnson, M. W. Wong, J. B. Foresman, M. A. Robb, M. Head-Gordon, E. S. Replogle, R. Gomperts, J. L. Andres, K. Raghavachari, J. S. Binkley, C. Gonzalez, R. L. Martin, D. J. Fox, D. J. Defrees, J. Baker, J. J. P. Stewart, and J. A. Pople, Gaussian, Inc., Pittsburgh, PA, 1993.

(8) (a) Hariharan, P. C.; Pople, J. A. *Theor. Chim. Acta* **1973**, *28*, 213. (b) Hariharan, P. C.; Pople, J. A. *Chem. Phys. Lett.* **1972**, *66*, 217. (c) Andzelm, J.; Klobukovski, M.; Radzio-Andzelm, E. *J. Comput. Chem.* **1984**, *5*, 146.

(9) Sosa, C.; Schlegel, H. B. *Int. J. Quantum Chem.* **1986**, *29*, 1001; **1987**, *30*, 155.

(10) The C−H bond length in methane, computed at various levels of theory with the 6-31G* basis set, is 1. 084 Å (HF), 1. 090 Å (MP2), 1. 085 Å (BHLYP), 1. 093 Å (B3LYP), and 1. 100 Å (BLYP). At the B3LYP level with the 6-31G** basis set the C−H distance becomes 1. 092 Å.

(11) (a) Kerr, J. A.; Timlin, D. M. *Int. J. Chem. Kinet.* **1971**, *3*, 427. (b) Golden, D. M.; Benson, S. W. *Chem. Rev.* **1969**, *69*, 125. (c) Furuyama, S.; Golden, D. M.; Benson, S. W. *J. Am. Chem. Soc.* **1969**, *91*, 7564. (d) Mendehall, G. D.; Golden, D. M.; Benson, S. W. *J. Phys. Chem.* **1973**, *77*, 2707.

(12) (a) Pross, A.; Schaik, S. S. *Acc. Chem. Res.* **1983**, *16*, 363. (b) Bernardi, F.; Olivucci, M.; McDouall, J. J. W.; Robb, M. A. *J. Chem. Phys.* **1988**, *89*, 6365.